AIAA–2002–0383

LEWICE 2.2 Capabilities and Thermal Validation

William B. Wright
QSS Group, Inc.
Cleveland, OH

40th Aerospace Sciences Meeting & Exhibit
January 8–11, 2002 / Reno, NV

AIAA–2002–0383

LEWICE 2.2 Capabilities and Thermal Validation

William B. Wright*
QSS Group, Inc.
Cleveland, Ohio 44135

I. Abstract

A computational model of bleed air anti-icing and electrothermal de-icing have been added to the LEWICE 2.0[1] software by integrating the capabilities of two previous programs, ANTICE[2] and LEWICE/Thermal[3]. This combined model has been released as LEWICE version 2.2. Several advancements have also been added to the previous capabilities of each module. This report will present the capabilities of the software package and provide results for both bleed air and electrothermal cases. A comprehensive validation effort has also been performed to compare the predictions to an existing electrothermal database. A quantitative comparison shows that for deicing cases, the average difference is 9.4°F (26%) compared to 3°F for the experimental data while for evaporative cases the average difference is 27°F (32%) compared to an experimental error of 4°F.

II. Nomenclature

A	Area(m^2)
C_e	Mass concentration of water in air at the edge of the boundary layer (kg/m^3)
C_p	Heat capacity (kJ/kgK)
C_s	Mass concentration of water in air at the surface (kg/m^3)
e	Evaporative pressure (N/m^2)
F	Force per unit span (N/m)
H	Enthalpy per unit volume (kJ/m^3)
h	Heat transfer coefficient ($kW/m^2°K$)
h_m	Mass transfer coefficient (m/s)
k	Thermal conductivity (kW/m°K)
L	Lewis number
L_f	Latent heat of fusion (kJ/kg)
L_v	Latent heat of vaporization (kJ/kg)
LWC	Liquid water content of air (kg/m^3)
M	Mach number
$\dot{m}$	Mass flux (kg/m^2s)
MW	Molecular weight (kg/kg mol)
N	Mass flux (kg/m^2s)
N_f	Freezing fraction
q"	Heat flux (kW/m^2)
q"'	Volumetric heat source (kW/m^3)
Pr	Prandtl number
R	Ideal gas constant (kJ/kg mol°K)
r	Recovery factor
T	Temperature (°K)
t	Time (s)
V	Velocity (m/s)
W_e	Weber number
x	Parallel to the airfoil surface (m)
y	Perpendicular to the airfoil surface (m)

Greek Letters

γ	Ratio of heat capacities C_p/C_v
ρ	Density (kg/m^3)

Subscripts

a	accretion
aero	aerodynamic
air	air
conv	convection
e	edge of boundary layer
evap	evaporation
fh	frictional heat
ice	ice
k	layer number
lat	latent heat
l	liquid phase
m	melt phase
nc	net amount of convection
o	total property
r	melt range
rec	recovery property
s	solid phase
w	water
x	x-dependent
y	y-dependent
∞	free-stream property

*Senior Member, AIAA.

III. Introduction

The removal and/or prevention of ice on aircraft components is vital to aircraft performance and operation. Even small amounts of ice can have disastrous consequences. Because of this, several methods of ice prevention and removal have been designed. Methods of ice control can be arranged into two broad categories: anti-icing methods and de-icing methods. Anti-icing methods are concerned with the prevention or minimization of ice buildup on protected surfaces. De-icing methods are concerned with ice removal after and during ice build up.

The primary means of preventing ice formation on wings and engine inlets for modern commercial transport aircraft is by extracting hot air from the compressor and blowing it on the inside surface of the leading edge through small holes drilled in a pipe. The amount of heat supplied is usually determined by correlations based upon hole and pipe diameter, the number of holes, the mass flow rate of the air and the supply temperature. Ice accretion is prevented by supplying enough energy to evaporate the impinging water (evaporative anti-icing) or by maintaining a surface temperature above freezing (running wet anti-icing).

Another widely used method for either anti-icing or de-icing aircraft components is with an electrothermal pad. By this method, heater mats are installed beneath the skin of a wing surface surrounding the leading edge as shown in Fig. 1. Thermal energy in the form of conducted heat melts a thin layer of ice which destroys the adhesion force at the ice-surface interface. Aerodynamic forces then sweep the ice from the surface. When more heat is supplied, the ice will melt completely and runback to unheated regions. If enough heat is supplied, the water will not freeze on the surface, creating an anti-icing condition similar to the bleed air case.

The report is divided into three sections. The first section will provide a description of LEWICE 2.2 model, with emphasis on the anti-icing and de-icing physics. The second section will provide several examples illustrating the capabilities of the bleed air anti-icing model, including design analysis performed for an IRT test scheduled in FY02. The third section will provide example cases and comparisons from the electrothermal model. A detailed comparison with experimental data is performed, an effort comparable in complexity and scale to the validation effort performed for LEWICE 2.0[4].

IV. LEWICE 2.2

The computer program LEWICE embodies an analytical ice accretion model that evaluates the thermodynamics of the freezing process that occurs when supercooled droplets impinge on a body. The atmospheric parameters of temperature, pressure, and velocity, and the meteorological parameters of liquid water content (LWC), droplet diameter, and relative humidity are specified and used to determine the shape of the ice accretion. The surface of the clean (un-iced) geometry is defined by segments joining a set of discrete body coordinates. The software consists of four major modules. They are 1) the flow field calculation, 2) the particle trajectory and impingement calculation, 3) the thermodynamic and ice growth calculation, and 4) the modification of the current geometry by addition of the ice growth.

LEWICE applies a time-stepping procedure to "grow" the ice accretion. Initially, the flow field and droplet impingement characteristics are determined for the clean geometry. The ice growth rate on each segment defining the surface is then determined by applying the thermodynamic model. When a time increment is specified, this growth rate can be interpreted as an ice thickness and the body coordinates are adjusted to account for the accreted ice. This procedure is repeated, beginning with the calculation of the flow field about the iced geometry, then continued until the desired icing time has been reached.

The thermal module calculates the 2D transient (time-dependant) heat transfer in a body. It can handle multiple composite layers, where each layer can have different thermal properties including temperature dependence and anisotropy. Each section can contain a heater which is individually controlled with separate on/off times and power densities. Ice growth can be predicted with or without heaters, and the model includes various modes for ice shedding and water runback. It can also function as an ice accretion simulator with heater power turned off. The original deicer program has been documented in previous reports[3,5]. For version 2.2, this module has been modified to include boundary conditions which model the heat flux or heat transfer coefficient from a bleed air system.

LEWICE 2.2 has been designed to combine the best features of LEWICE 2.0, LEWICE/Thermal and ANTICE. It incorporates the multi-time stepping capabilities of LEWICE as well as the ability to easily interface with other software. It contains the flexibility in heater design and materials from LEWICE/Thermal and incorporates the bleed air analysis and rivulet runback capabilities found in ANTICE.

V. Thermal model description

The following assumptions were made in the development of a mathematical model for heat conduction in a composite airfoil:

1. The thermal physical properties of the material composing each layer of the airfoil may be different.

2. Each layer is either isotropic or orthotropic, meaning that cross-derivative terms in the anisotropic heat equation are neglected, but that thermal conductivity with the grain can be different from the thermal conductivity against the grain of the material.

3. There is perfect thermal contact between layers.

4. The thickness of each layer can be assumed constant in the chordwise direction.

5. Curvature effects of the airfoil are not taken into account because the deicer thickness normal to the airfoil is thin compared to the effective airfoil thickness.

This assumption does not mean that curvature effects are unimportant nor that curvature effects are ignored. The assumption is that body curvature only effects the air flow, the collection efficiency, the convective heat transfer and the ice shape. The conduction heat transfer can be modeled as a two-dimensional rectangular entity if the deicer is thin compared to the airfoil. This is usually true, since a thick deicer is not very efficient.

6. Heat transfer in the spanwise direction is negligible.

7. The ambient conditions (temperature, velocity, etc) are constant with respect to time.

8. The phase change of the ice is assumed to occur over a small temperature interval near the true melting point rather than at the melting point itself.

With the above assumptions, the mathematical formulation for the problem of unsteady heat conduction in a chord-wise two-dimensional composite airfoil with electrothermal heating can be represented as:

$$(\rho C_p)_k \frac{\partial T}{\partial t} = k_{x,k}\frac{\partial^2 T}{\partial x^2} + k_{y,k}\frac{\partial^2 T}{\partial y^2} + q'''_k \qquad (1)$$

For the ice layer, the governing equation in terms of the enthalpy is given by

$$\frac{\partial H}{\partial t} = k_{ice}\left(\frac{\partial^2 T}{\partial x^2} + \frac{\partial^2 T}{\partial y^2}\right) \qquad (2)$$

In order to solve this problem, it is necessary to remove enthalpy from the governing equation above and replace it with temperature. The standard relationship between enthalpy and temperature is

$$H = \begin{bmatrix} (\rho C_p)_s T \\ (\rho C_p)_s T_m < H < \rho_l C_{ps} T_m + \rho_l L_f \\ (\rho C_p)_s T_m + \rho_l L_f + (\rho C_p)_l (T - T_m) \end{bmatrix} \begin{bmatrix} T < T_m \\ T_m \\ T > T_m \end{bmatrix} \qquad (3)$$

However, this relationship is nonlinear, as there are multiple values for the enthalpy while the temperature remains at the melting temperature. The numerical method employed requires that a linear relationship exists, so that the coefficient matrix created can be easily inverted. To accomplish this, ice is assumed to melt over a very small temperature range near the melting temperature instead of at the melting temperature. The modified form of the enthalpy/temperature relationship is:

$$H = \begin{bmatrix} (\rho C_p)_s T \\ \rho_m C_{ps} T_m + \rho_m L_f \dfrac{(T - T_m)}{T_r} \\ \rho_l C_{ps} T_m + \rho_l L_f + (\rho C_p)_l (T - T_m - T_r) \end{bmatrix} \begin{bmatrix} T < T_m \\ T_m < T < T_m + T_r \\ T > T_m + T_r \end{bmatrix} \qquad (4)$$

It is convenient to define a specific heat capacity in this melt region, which is given by:

$$(C_p)_m = \frac{(\rho_l - \rho_s) C_{ps} T_m + \rho_l L_f}{\rho_m T_r} \qquad (5)$$

where ρ_m is the density of the region between solid and liquid, henceforth to be referred to as the 'melt' region. Therefore, the governing equation for the ice layer can be written as:

$$\begin{bmatrix} \frac{\partial}{\partial t}(\rho_s C_{ps} T) \\ \frac{\partial}{\partial t}(\rho_m C_{pm} T) \\ \frac{\partial}{\partial t}(\rho_l C_{pl} T) \end{bmatrix} = \frac{\partial}{\partial x} k_{ice} \frac{\partial T}{\partial x} + \frac{\partial}{\partial y} k_{ice} \frac{\partial T}{\partial y} + \tag{6}$$

$$\begin{bmatrix} 0 \\ \left[(\rho C_p)_m - (\rho C_p)_s\right] T_m \\ \left[(\rho C_p)_l - (\rho C_p)_s\right] T_m + \left[(\rho C_p)_l - (\rho C_p)_m\right] T_r \end{bmatrix}$$

where the top expression in each bracket is used for the solid phase, the middle expression is used for the melt phase, and the bottom expression is used for the liquid phase. As long as this range is small, the accuracy of the solution is not significantly altered. A melting range of 10^{-4}K or smaller has proven to be necessary for this application. Since the temperature is not known prior to this calculation, the phase of the ice (solid, melt, or liquid) must first be assumed, the temperature calculated using the appropriate equation, and the phase checked at the end. This creates an iterative scheme to solve for the temperature within the composite body.

Boundary Conditions

There are four types of boundary conditions used for the composite body. They are:

1. Interior interfaces between layers of the composite body.
2. Fixed temperature outer boundary conditions.
3. Convection outer boundary conditions.
4. Heat flux outer boundary conditions.

At interior interfaces, the temperatures and heat fluxes are continuous, i.e.:

$$T)_{layer1} = T)_{layer2} \tag{7}$$

$$-k_x \frac{\partial T}{\partial x}\Big)_{layer1} = -k_x \frac{\partial T}{\partial x}\Big)_{layer2} \tag{8}$$

$$-k_y \frac{\partial T}{\partial y}\Big)_{layer1} = -k_y \frac{\partial T}{\partial y}\Big)_{layer2} \tag{9}$$

where Eq. 8 or Eq. 9 is used depending upon whether the interface in question is in the x-direction or in the y-direction.

Fixed temperature interfaces are given by:

$$T)_{surface} = T_\infty \tag{10}$$

or

$$T)_{surface} = T_{rec} \tag{11}$$

Equation 10 is rarely used for the simulation of a de-icer pad, but has been incorporated into the program which has been developed so that other heat transfer phenomena may be studied by the user. Equation 11 can be used to model a dry air boundary condition.

Convection boundary conditions are given by:

$$-k_x \frac{\partial T}{\partial x}\Big)_{surface} = h(T_s - T_\infty) \tag{12}$$

$$-k_y \frac{\partial T}{\partial y}\Big)_{surface} = h(T_s - T_\infty) \tag{13}$$

Insulated boundary conditions are obtained by setting the heat transfer coefficient in the above equations to zero. Additionally, the heat transfer coefficient can be constant or more likely a function of position on both the external boundary and on the internal boundary when analyzing a bleed air case.

Heat flux boundary conditions are given by:

$$-k_x \frac{\partial T}{\partial x}\Big)_{surface} = q_s \tag{14}$$

$$-k_y \frac{\partial T}{\partial y}\Big)_{surface} = q_s \tag{15}$$

The heat flux can also be given as a function of position as would be the case when performing a bleed air analysis. The final type of boundary condition used at the top surface of the ice, and it is derived in the next section.

Accretion Boundary Condition

In early numerical models of a de-icer pad, the outer boundary condition at the top surface of the ice was assumed to be given by Eq. 12 of the previous section. However, this is not adequate when the

actual physics of the flow at the exposed surface are considered. The approach used here is a modified version of the approach used in the LEWICE model[1] and by Gent and Cansdale[6]. There are several assumptions which need to be made in the development of an improved icing boundary condition. These are listed below.

1. The terms in the energy equation which are considered important are:
   a. convection losses.
   b. kinetic heating.
   c. evaporative/sublimative cooling.
   d. sensible heat gain/loss.
   e. viscous losses.
   f. latent heat gain.
   g. conduction into or out of the body
   All other terms are neglected.
2. Kinetic heating is adiabatic.
3. The Chilton-Colburn analogy is used to relate the mass loss caused by evaporation to a heat loss caused by evaporation.
4. Viscous dissipation is given by a 'recovery factor' as defined by Schlichting[7].
5. Air is a perfect gas.
6. The Antoine equation is used to relate vapor pressure to static temperature. This implies that the molar volume of the liquid is negligible compared to that of the gas and that the heat of evaporation is independent of temperature.
7. Physical properties of air and water, except for air density, are independent of temperature.
8. Mass transfer is proportional to the concentration difference across the boundary layer.
9. The ambient conditions of velocity and mass density are constants.

If dry air flows over the airfoil, the surface temperature would be increased beyond that of the ambient because of the compressible flow of air which strikes the surface of the airfoil, thereby imparting the kinetic energy of the air to the airfoil. Since this is presumed to be an adiabatic process, the local static temperature at the edge of the boundary layer would be given by:

$$T_e = \frac{T_o}{\left(1 + \frac{\gamma - 1}{2} M_e^2\right)} \tag{16}$$

Schlichting relates this temperature to the surface temperature through the 'recovery factor' r which is equal to $Pr^{1/3}$ for a turbulent boundary layer and $Pr^{1/2}$ for a laminar boundary layer. This is presumed to account for the viscous dissipation in the boundary layer. The final result is called the recovery temperature and is given by:

$$T_{rec} = \frac{T_o\left(1 + r\frac{\gamma - 1}{2} M_e^2\right)}{\left(1 + \frac{\gamma - 1}{2} M_e^2\right)} \tag{17}$$

where T_{rec} is the recovery temperature. The amount of energy increase owing to the combined effects of the frictional heating by air and the viscous dissipation of the boundary layer is normally placed in terms of a convective flux:

$$q''_{fh} = h(T_{rec} - T_\infty) \tag{18}$$

The convective flux is described by Newton's Law of Cooling:

$$q''_{conv} = h(T_s - T_\infty) \tag{19}$$

When convection is combined with frictional heating, Eqs. 18 and 19 may be united into a net convective flux which is given by:

$$q''_{nc} = h(T_s - T_{rec}) \tag{20}$$

An additional kinetic heating term is also present owing to the impact of the water droplets on the surface. This is given by:

$$q''_{ke} = \frac{\dot{m}_w V_\infty^2}{2} \tag{21}$$

The heat loss caused by evaporation is determined by finding the mass transfer rate of water vapor leaving the surface of the airfoil and multiplying it by the heat of vaporization. Sublimation is handled in the same manner, but using the heat of sublimation. Since the latent heats of vaporization and sublimation are large, it takes only a small amount of mass to be removed by either process before a significant drop in surface temperature is realized. The driving force for this process is the concentration difference across the boundary layer, C_s-C_e, where the mass density, C, is given by:

$$C = \frac{e(MW)_w}{RT} \tag{22}$$

The evaporative mass flux of water vapor through the boundary layer can be described by:

$$N = h_m(C_s - C_e) \tag{23}$$

The heat loss is given by:

$$q''_{evap} = L_v N \tag{24}$$

Combining Eqs. 22 through 24, the evaporative heat loss can be written as:

$$q''_{evap} = \frac{L_v h_m (MW)_w}{R}\left(\frac{e_s}{T_s} - \frac{e_e}{T_e}\right) \tag{25}$$

The mass transfer coefficient can be replaced with the heat transfer coefficient via the Chilton-Colburn analogy[8] between heat and mass transfer:

$$h_m = \frac{h}{(\rho C_p)_{air} L^{2/3}} \tag{26}$$

Replacing the density of air via the ideal gas law gives the net heat lost by evaporation as:

$$q''_{evap} = \frac{L_v h (MW)_w}{[P_o (MW) C_p]_{air} L^{2/3}}\left(e_s \frac{T_e}{T_s} - e_e\right) \tag{27}$$

The evaporative pressure at any location can be evaluated solely in terms of the local static temperature using Antoine's equation:

$$\log e_s = A - \frac{B}{T_s + C} \tag{28}$$

where A, B, and C are empirical constants. Since the temperature at the edge of the boundary layer is given by Eq. 13 and the evaporative pressure is given by Eq. 25, the only unknown in Eq. 27 is the surface temperature.

The sensible heat transfer and the latent heat transfer are determined by tracing the thermodynamic path the incoming liquid takes to get to the surface temperature. The exact form of these equations depends upon how much heat is available after the other heat losses/gains have been considered. If the surface temperature is below the freezing point, the sensible and latent heat terms needed are the heating of the supercooled liquid up to freezing, the freezing of the water into ice (latent heat), and the subsequent cooling to the surface temperature. These three terms can be expressed in equation form as:

$$q''_{sens1} = -\dot{m}_w C_{pl}(T_m - T_\infty) \tag{29}$$

$$q''_{lat} = \dot{m}_w L_f \tag{30}$$

$$q''_{sens2} = -\dot{m}_w C_{ps}(T_s - T_m) \tag{31}$$

If the surface is at the freezing point and hence only part of the ice freezes, the terms are the heating of the supercooled liquid up to freezing and the partial freezing of the water into ice (latent heat). These terms can be described by:

$$q''_{sens3} = -\dot{m}_w C_{pl}(T_m - T_\infty) \tag{32}$$

$$q''_{lat} = N_f \dot{m}_w L_f \tag{33}$$

Since the assumption has been made that ice melts over a small temperature range, the freezing fraction can be written in terms of the surface temperature:

$$N_f = \frac{T_m + T_r - T_s}{T_r} \tag{34}$$

Hence, the latent heat term for this case can be written as:

$$q''_{lat} = \frac{(T_m + T_r - T_s)\dot{m}_w L_f}{T_r} \tag{35}$$

If the surface temperature is above freezing, the sensible heat is given by:

$$q''_{sens1} = -\dot{m}_w C_{pl}(T_s - T_\infty) \tag{36}$$

Additionally, there is a sensible heat transfer between the runback water and the region into which the water flows. This heat exchange is caused by the temperature distribution along the airfoil. These terms cannot be discounted, as they are quite significant for cases involving a considerable amount of runback. The form of the equations describing this sensible heat transfer is the same as those for the sensible heat terms above, but replacing $\dot{m}_w$ with the mass flux of runback water, $\dot{m}_{rb}$, and the ambient

temperature, T_∞, with the temperature of the runback water, T_{rb}.

The accretion boundary condition can be found by setting the heat flux at the outer surface equal to the sum of the heat fluxes described above. This can be written as:

$$-\left(k_y \frac{\partial T}{\partial s}\right)_s = q''_{nc} + q''_{evap} - q''_{ke} - q''_{lat} \pm q''_{sens} \quad (37)$$

Note that the heat flux is directed outward, such that a term which results in a heat gain at the surface has a negative sign and a term which results in a heat loss has a positive sign. As with the governing equations for conduction within the de-icer, the surface temperature is not known prior to this calculation, so that the Method of Assumed States must be used here as well.

Accretion Mass Balance

In the previous section, conservation of energy was applied at the top surface of the ice. This resulted in the derivation of an appropriate boundary condition for the heat conduction equation. In this section, conservation of mass will be applied to the same surface to determine the amount of ice which forms on the airfoil. The additional assumptions which have been made in this derivation are:

1. The flow of surface water is shear driven. Hence if all of the incoming water does not freeze it will build up at that control volume until the aerodynamic forces become larger than the surface tension force, which will cause flow into the next control volume as runback water.

2. Runback water flows in the direction opposed to the aerodynamic stagnation point. Because of this, no runback water can flow into the control volume which contains the stagnation point.

3. Any runback water which the stagnation point control volume generates is equally divided into the two control volumes on each side of this point.

Because of the above assumptions, the mass balance must be applied to the stagnation point control volume first, as the amount of runback water present elsewhere is dependent upon the amount generated at the stagnation point. The general form of the mass balance in terms of the mass fluxes is:

$$\dot{m}_w + \dot{m}_{rb,in} = \dot{m}_e + \dot{m}_a + \dot{m}_{rb,out} + \dot{m}_{sh} + \dot{m}_r \quad (38)$$

The mass flux of impinging water is given by:

$$\dot{m}_w = \beta(LWC)V_\infty \quad (39)$$

The collection efficiency (β) given above is simply the fraction of water droplets in a volume of water which impinges upon the surface, meaning that the droplet strikes the surface and remains there and does not splatter. The collection efficiency can be obtained by correlations with the ambient conditions, or by a separate computer program which calculates the trajectory of the droplets in the air and determines if they will strike the surface and if so, if they will splatter or remain upon the surface. The collection efficiency is calculated by trajectory module in LEWICE 2.2.

The mass lost by water shedding is determined independently from the other mass balance terms and is based on the Weber number. Water shedding can occur from runback watter being sheared from a horn or by removal of existing surface water by shashing of incoming drops. The amount of water shedding is assumed to encompass both water shedding and water splashing as both are considered to be controlled by the Weber number. The empirical expression for the amount lost is given by

$$\dot{m}_{sh} = \dot{m}_w \left(\frac{W_e - W_{e,c}}{W_e}\right) \quad (40)$$

where W_e is the Weber number of the runback bead and $W_{e,c}$ is the critical Weber number to initiate shedding. A value of $W_{e,c} = 500$ is currently used. If the Weber number is less than $W_{e,c}$ then no mass is lost by water shedding.

The term $\dot{m}_r$ is the amount of unfrozen water which is not allowed to leave the control volume due to surface tension (Weber number) effects. The runback velocity is assumed to be 1/2 of the local air velocity at the edge of the boundary layer. The value of 1/2 was determined by assuming the water flow is shear driven. If the mass flux of water computed to runback is more than the flux computed using this velocity, the remaining water is kept at that control volume until the next time step.

The mass flux of evaporation is given by:

$$\dot{m}_e = \frac{q''_{evap}}{L_e} \quad (41)$$

One of the purposes of equations in the previous section was to obtain the freezing fraction, N_f. This is the fraction of impinging water which freezes. Hence, the amount of runback water leaving the control volume is obtained by multiplying the total amount of incoming water by the fraction which does not freeze. Hence:

$$\dot{m}_r + \dot{m}_{rb,\,out} = (\dot{m}_w + \dot{m}_{rb,\,in})(1 - N_f) \qquad (42)$$

The mass flux of runback water coming in, $\dot{m}_{rb,\,in}$, is zero at the stagnation point and is calculated from the previous volume's mass balance elsewhere. This is why it is necessary to start the calculations at the stagnation point. The right-hand side of this equation is compared to the maximum runback mass flux, $\rho_l V_e/2$. If the amount of available water is more than the maximum, the excess water is stored in m_r until the next time step. The mass flux of ice accretion is obtained by solving Eq. 38 for $\dot{m}_a$ and substituting the above expressions to obtain:

$$\dot{m}_a = (\dot{m}_w - \dot{m}_{rb,\,in})N_f - \frac{q''_{evap}}{L_e} - \dot{m}_{sh} \qquad (43)$$

Ice Shedding

The assumptions made in the development of an ice shedding model are:

1. The flow is two-dimensional, that is, the aerodynamic force has x and y-components only.
2. The forces holding the ice to the surface are determined from the bonding strength of the ice.
3. The bonding strength is dependant only upon the temperature at the ice/airfoil interface.
4. The ice can shed as a whole or in sections.
5. Each spanwise section acts independently of the other sections.
6. The ice will shed when the net average external forces exceed the net average force holding the ice to the surface. The aerodynamic force is computed from the flow solution as either a macroscopic force over the whole airfoil or at each individual location, depending on the shedding mechanism chosen by the user.

The equations relating bonding strength of the ice versus temperature were obtained by curve-fitting experimental data provided by Scavuzzo[9]. The computational domain takes the x-direction to be along the surface of the airfoil in the chordwise direction. The y-direction is normal to the airfoil, and the z-direction is along the surface of the airfoil in the spanwise direction. Shedding ice as a whole assumes that the tensile strength of ice is very high. This means that if part of the ice adheres to the surface, all of the ice will remain. Shedding by node assumes that ice has no tensile strength. This means that if the adhesive strength at that location goes to zero (the ice melts) then it can not be held in place by the neighboring nodes. Prediction of surface temperatures and shedding times from the experimental data set indicate that the second assumption is more likely for the conditions tested.

VI. Bleed Air Results

The bleed air design used for this analysis is shown in Fig. 2. It was designed by Jim Van Fossen and Phil Poinsette from the NASA Glenn Heat Transfer Branch based upon their experience with turbine blade cooling. Some examples of their previous work have been provided for reference[10-13]. The model was designed for use as a validation model and was not intended to represent any existing design used by industry.

The exterior surface is a NACA0012 airfoil, shown in Fig. 3. The interior surface has a uniform channel with small holes at the chordwise locations shown in Fig. 2. The holes were 0.045" in diameter and were spaced 10 diameters, or 0.45" apart. A benchtest was performed using liquid crystals to determine the heat transfer coefficients on the inside surface[14]. A sample heat transfer curve from this test is shown in Fig. 4. This model will be tested in FY02 in the IRT. An example output for an evaporative condition from the test matrix is shown in Fig. 5.

A second example case uses five 2D cross sections of an engine inlet as the body geometries. The first of these cross-sections is shown in Fig. 6. This model was taken from a LEWICE3D[15] example case provided by Colin Bidwell. The surface pressure coefficients, collection efficiencies, and external heat transfer coefficients were supplied from a LEWICE3D output file at each 2D cross-section shown. The internal heat transfer coefficients for this case were selected such that residual ice would form. A plot of these values are shown in Fig. 7. These values were then used for each cross-section. Since the inputs

and results for each cross-section are very similar, only the inputs and results for the first section are shown in this paper. The LEWICE 2.2 draft user manual provides additional analysis of this case. Figure 8 shows surface temperature predictions for the first section. The temperatures and the resultant residual ice, shown in Fig. 9, can then be loaded back into LEWICE3D for the generation of a simulated 3D residual ice shape. The simulated 3D ice shape is shown in Figure 10. The resolution of the ice shape in this figure can be improved by the addition of more streamlines to the model or by interpolation from the existing results. Since LEWICE 2.2 also contains a prediction of rivulet formation in its model, it should be possible in the future to display that information as well.

VII. Electrothermal Validation

The test article used to generate the electrothermal deicer database was a NACA0012 airfoil with a 72 inch span and a 36 inch chord. The leading edge had seven independently controllable heater zones as shown in Fig. 11. The material properties of the heater mat are given in Table 1. Heater zone A (parting strip) was on continuously for all the runs. The other heaters were cycled using various power settings and on/off times. Results from this test were previously reported[15].

Development of the test matrix involved the selection of two different types of parameters: icing parameters (T_o, LWC, MVD, etc.) and electrothermal ice protection system parameters (heater power level and heater zone on/off time). The combination of both sets of parameters resulted in an extremely large number of possible test parameter combinations. Consequently, the test was restricted to a few variations in icing conditions and a wider variety of ice protection parameters. Including repeat runs, there were 113 runs in this test entry.

For each data point, three LEWICE 2.2 outputs were generated. In the first set of cases, the program used the standard external heat transfer coefficient which is calculated for icing runs. A second set of outputs were generated using a laminar heat transfer coefficient on the external boundary. This assumption argues that the airfoil surface is kept relatively clean by the de-icer, therefore the boundary layer will remain laminar within the impingement limits (natural transition normally occurs further downstream). The third set of comparisons used the laminar boundary layer assumption as well as an assumption of zero tensile strength for the ice, allowing each node of ice to shed independently of the other. The first two sets of output assumed that the ice shed in sections. All of these cases have been compared to the LEWICE 2.2 model.

Figure 12 shows the comparison on the parting strip for Run17 from the test matrix using the standard boundary layer transition model. This plot shows the comparison for an RTD (resistance temperature device) located below the heater. Figures 13 and 14 show results comparing thermocouples at the surface and on the inside surface of the airfoil. Figures 15-20 show the comparisons for sections "B" and "D" for the same run. The quality of this comparison is typical for the deicing cases in this matrix. Since the model is symmetric, only data from one side needs to be shown. The fluctuations in the experimental results for section "A" occur when section "B" and "C" heaters are on. This effect does not occur numerically due to the underprediction of those temperatures. The conditions for this case, including heater power and cycle times, is shown in Table 2.

This comparison shows that section "A" is well predicted, while the other zones are underpredicted. This result occurred because section "A" is in the laminar region of the boundary layer while the other zones see the effects of the higher turbulent heat transfer coefficient. Therefore, the case was run using a laminar boundary layer assumption. The results for this case are shown in Figs. 21-29. Figures 21-23 show the output for section "A". Although the boundary layer is laminar for the previous case as well, this case has a higher temperature as less heat is lost to the other sections. Figures 24-29 show a larger increase in temperature due to the change in assumption. Although the temperatures are slightly overpredicted, the comparison has improved significantly. Once again, this result is typical for a large majority of de-icing cases. A minority of cases still show an underprediction even with the laminar assumption.

The last set of comparisons uses an alternative shedding mode than the previous runs. The previous runs allowed ice to shed only section by section, meaning that any ice which would accumulate could only shed if the aerodynamic force exceeded the adhesion force over the entire section. The sectional

shedding model is a new feature not modeled by previous deicer programs. LEWICE/Thermal could shed ice an a whole or by each node acting independently. This latter assumption was used in the third set of comparisons in order to assess its value. For brevity, only the heater temperatures are shown. Figures 30-32 show the results of using this assumption. While the comparisons are similar to those obtained with the sectional shedding model, the latter heater cycles show a tendency of the nodal shedding cases to increase the peak temperature. Once again, these results are fairly typical for cases ran using this assumption.

VIII. Quantitative Analysis

The previous section used a qualitative analysis to compare outputs from LEWICE 2.2 to the experimental data. This section will describe a methodology which was created to quantify those findings. The first step in this process was to create a version of the software that runs in batch mode. In this mode, interactive inputs were automatically answered so that the user did not need to be at the display entering filenames. This mode is not recommended for standard use, as the warning and error messages displayed often point to input file errors. Second, a script was written to run each of the 113 cases sequentially, along with a small data reduction program that converted temperatures to Fahrenheit and reduced the output to one value per second to match the experimental data.

The third step involved writing a Visual Basic® program in Microsoft Excel®. In this step, each second of experimental data was compared to each second of computational output, with the absolute difference and absolute percent differences calculated for each comparison. The macro also produced the comparison plots shown earlier. These steps greatly reduced the man-hours necessary to produce a comprehensive comparison which allowed the exploration of alternative assumptions shown previously. The average differences and percentage differences for each thermocouple reading were then averaged for that case and finally the results for each case were averaged. The differences and percent differences were calculated by the following equations:

$$abs\ difference = |T_{\exp} - T_{LEWICE}| \quad (44)$$

$$abs\ percent\ difference = \frac{100|T_{\exp} - T_{LEWICE}|}{T_{\exp\ max} - T_{\exp\ min}} \quad (45)$$

Table 3 shows a summary of results from the quantitative analysis. There are 69 cases which reside under the de-icing category. While the overall results are similar for the three sets of comparisons, it should be noted that both laminar comparisons resulted in an overprediction of temperatures while the turbulent cases resulted in an underprediction of temperatures. This result indicates that it would be possible to produce a calibrated external heat transfer coefficient which would more accurately predict the experimental temperatures. This calibration was not performed, as the purpose of the validation was to show the comparison capabilities using current capabilities only. This table also shows that the percentage difference between LEWICE 2.2 and experiment is not a function of the ambient temperature and that a larger temperature difference is obtained for colder conditions which have more power applied to them. This result is consistent with the conclusion that a calibrated heat transfer coefficient could be derived from the experimental results.

There were 44 cases which had power supplied continuously to all of the heaters. Of these cases, 17 were run with a high enough power setting to evaporate all of the incoming water. The other 27 cases had runback ice past the heater zones. Table 3 also shows the predictive capability of LEWICE 2.2 for these cases. Although the average absolute difference for these cases was extremely high, the average absolute percentage difference using the laminar assumption is similar to the de-icing cases. In this case however, a calibrated heat transfer coefficient can not be derived. The laminar assumption with sectional shedding cases resulted in exactly 50% of the 44 cases being underpredicted and 50% over predicted. The nodal shedding assumption increased the number over predicted to 53%. For the turbulent assumption, 23% were over predicted with 77% underpredicted. There may be several factors which could explain both the poor prediction of the temperatures as well as their inconsistency.

The main cause appears to be that while the LEWICE 2.2 results were ran with a constant power setting, none of the experimental cases were ran in that mode. The power was continually adjusted both manually and with a temperature controller to obtain

a desired temperature response. Figure 33 shows the power input for Section A of Run 35A as a typical example. Experimentally, the power varied widely for the first part of the run, then was stabilized except for a period of time where it appears the power was accidentally turned off. LEWICE 2.2 cannot model this type of heater input. All of the LEWICE 2.2 cases were ran with a constant power setting at the level at which the power stabilized. The comparison was then made between experiment and LEWICE 2.2 only in the stabilized region. Despite these efforts, the temperatures were not well predicted for most of the evaporative cases.

IX. Ice Shape Validation

A quantitative analysis similar to the LEWICE 2.0 validation effort was also performed with this version of the software. A script similar to the one used for de-icing comparison was generated to reduce the time necessary for this effort. In this effort, the terms calculated are the same as those described in the validation report[4] with two exceptions. First, the upper and lower horn angles are now calculated relative to the leading edge of the clean airfoil and not to the center of the inscribed circular cylinder. The new definition is illustrated in Fig. 35. Second, the ice area is calculated by the following equation:

$$Area = (\int y \ dx)_{iced} - (\int y \ dx)_{clean} \qquad (46)$$

In order to compare these results to the experimental database and to LEWICE 2.0, these parameters were determined from the previous results. This operation was performed using similar scripts to those generated earlier. The results of this comparison are shown in Table 4. While the overall comparison of LEWICE 2.0 and LEWICE 2.2 results to experiment produce virtually identical results as shown in this table, individual cases can produce somewhat different ice shapes. Additionally, it is worthwhile mentioning that the automated process used here produced different values for each parameter when it was ran using LEWICE 2.0 than the values obtained from the LEWICE 2.0 validation report. Therefore, the automated process may not be an accurate assessment of the software's capabilities for ice shape generation.

X. Conclusions

Results to date have shown a reasonable comparison with deicing cases which have been analyzed. The results show that it would be possible to create a calibrated heat transfer coefficient which would better predict the experimental data. Evaporative cases are not well predicted with either the laminar or turbulent assumption. The turbulent cases have shown significant underprediction of temperature while the laminar cases show an overprediction in half of the cases. Ice shapes generated with LEWICE 2.2 have been shown to be quantitatively similar to the LEWICE 2.0 results, although the findings to date have been limited in scope.

XI. References

1 Wright, W. B., "Users Manual for the NASA Lewis Ice Accretion Code LEWICE 2.0," NASA CR 209409, Jan. 1999.

2 Al-Khalil, K.M., Miller, D. and Wright, W.B., "Validation of NASA Thermal Ice Protection Computer Codes: Part 3 - Thermal Anti-Icing," AIAA-97-0051, Jan. 1997.

3 Masiulaniec, K. C. and Wright, W. B., "User's Manual for the NASA Lewis Ice Accretion/Heat Transfer Prediction Code with Electrothermal Deicer Input", NASA CR 4530, 1994.

4 Wright, W. B. and Rutkowski, A., "Validation Results for LEWICE 2.0," NASA CR 208690, Nov. 1998.

5 Wright, W.B., Al-Khalil, K.M., and Miller, D., "Validation of NASA Thermal Ice Protection Computer Codes: Part 2 - Thermal De-Icing," AIAA-97-0050, Jan. 1997.

6 Gent, R.W., and Cansdale, J.T.: One-Dimensional Treatment of Thermal Transients in Electrically Deiced Helicopter Rotor Blades. Technical Report 80159, Royal Aircraft Establishment, Procurement Executive, Ministry of Defense, Farnborough, Hunts, England, 1980.

7 Schlichting, H.: Turbulent Boundary Layers in Compressible Flow. Boundary-Layer Theory, F. J.

Cerra, ed. Ch. XXIII, McGraw-Hill, New York, New York, 1979, pp. 713-715.

8 Bird, R.B., Stewart, W. E., and E. N. Lightfoot, Transport Phenomena, John Wiley & Sons, Inc., New York, 1960,pp. 647.

9 Scavuzzo, R. J. and Chu, M. L.: Structural Properties of Impact Ices Accreted on Aircraft Structures. NASA CR 179580, 1987

10 VanFossen, G. J. Simoneau, R. J., "Stagnation region heat transfer: The influence of turbulence parameters, Reynolds number and body shape," NASA-TM-106504, June 1994.

11 Masiulaniec, K. C., VanFossen, G. J., Dewitt, K. J., Dukhan, N., "Experimental technique and assessment for measuring the convective heat transfer coefficient from natural ice accretions," NASA-TM-106864, Jan. 1995.

12 Thurman, D., Poinsatte, P., "Experimental Heat Transfer and Bulk Air Temperature Measurements for a Multipass Internal Cooling Model with Ribs and Bleed," NASA/TM-2000-209772, May 2000.

13 Poinsatte, P., "Heat transfer measurements from a NACA 0012 airfoil in flight and in the NASA Lewis icing research tunnel," NASA-CR-4278, Mar. 1990.

14 Poinsatte, P., Internal NASA test using Liquid Crystal Technique (unpublished).

15 Bidwell, C.S., and Potapczuk, M.G., "Users Manual for the NASA Lewis Three Dimensional Ice Accretion Code (LEWICE3D)," NASA TM-105974, Dec. 1993.

16 Miller, D., Wright, W.B., and Al-Khalil, K.M., "Validation of NASA Thermal Ice Protection Computer Codes: Part 1 - Program Overview," AIAA-97-0049, Jan. 1997.

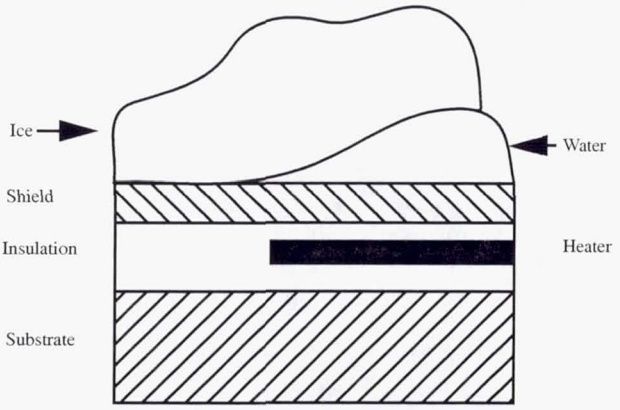

FIGURE 1. Representation of a Simple Deicer Model

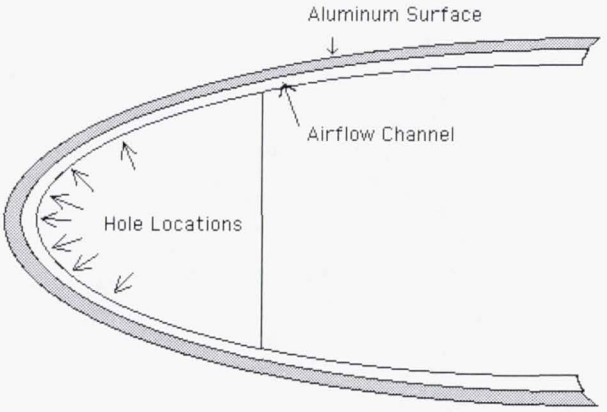

FIGURE 2. Validation Model Using Bleed Air

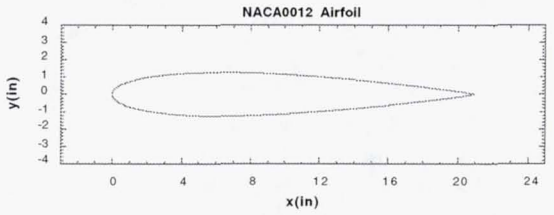

FIGURE 3. NACA0012 Airfoil

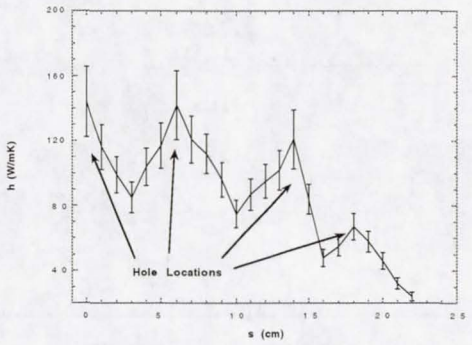

FIGURE 4. Experimental Heat Transfer Coefficients for Bleed Air Model

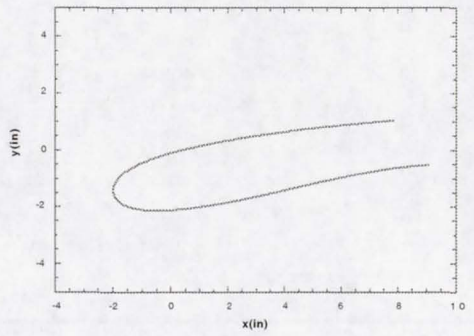

FIGURE 6. Engine Inlet Cross-Section

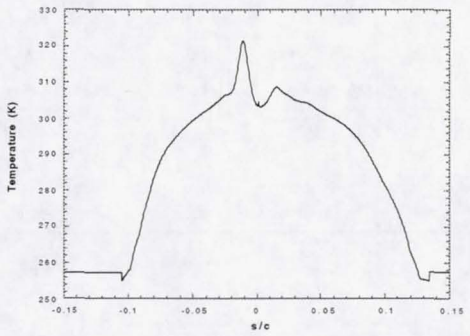

FIGURE 5. Predicted Temperature Distribution for Evaporative Bleed Air System

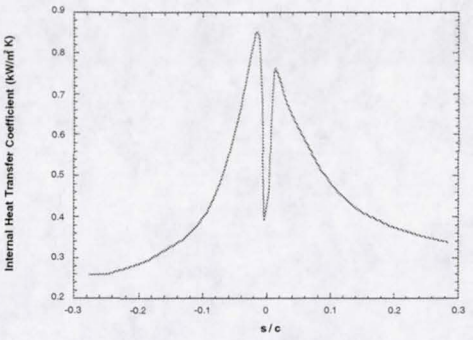

FIGURE 7. Bleed Air Heat Transfer Coefficients for Engine Inlet Model

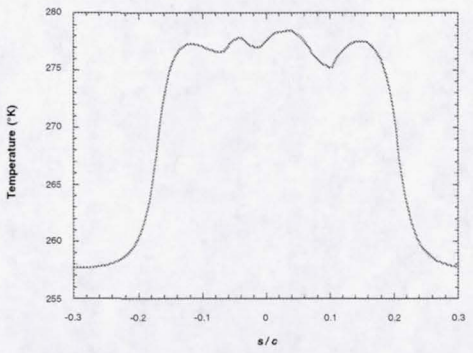

FIGURE 8. Surface Temperature Distribution for Engine Inlet Cross-section

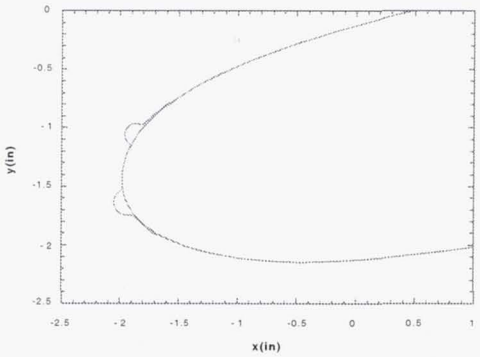

FIGURE 9. Residual Ice Shape for Engine Inlet Cross-section

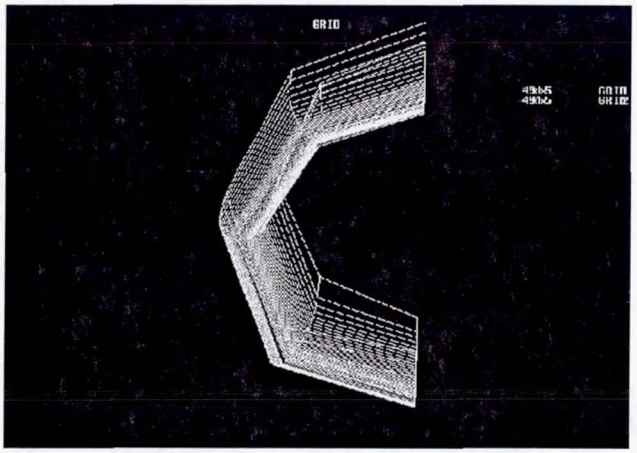

FIGURE 10. Simulated 3D Ice Accretion for Engine Inlet Half-Model

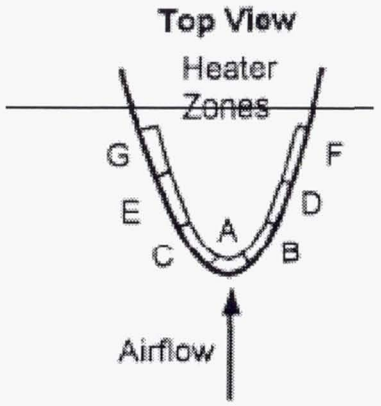

FIGURE 11. Schematic of Heater Zones

TABLE 1. Properties and Thicknesses of Deicer Pad

#	Material	Thickness (mm)	Conductivity (W/m/K)	Diffusivity ($m^2/s*10^7$)
1	Foam	3.43	0.121	1.65
2	Fiberglass	0.89	0.294	1.04
3	Elastomer	0.28	0.256	1.50
4	Heater	0.013	41.0	120.0
5	Elastomer	0.28	0.256	1.50
6	Ab. shield	0.20	16.3	40.6

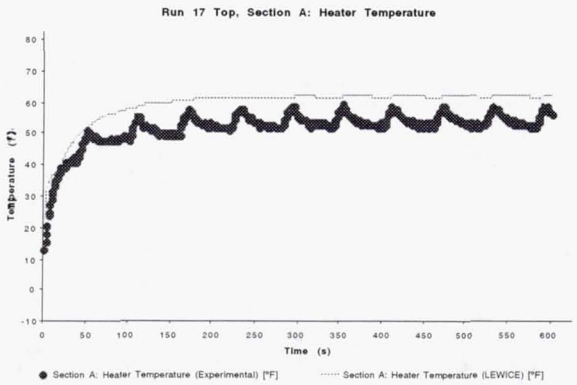

FIGURE 12. Turbulent Parting Strip Heater Temperature Comparison for Run17

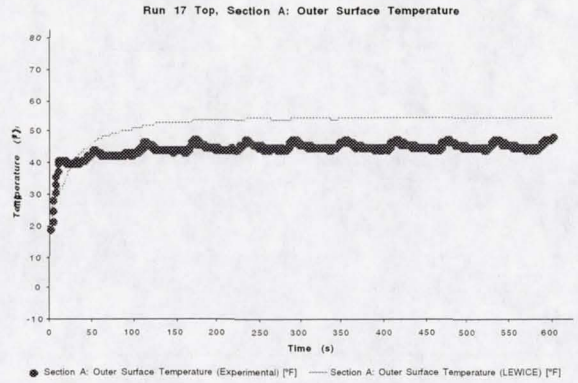

FIGURE 13. Turbulent Parting Strip Surface Temperature Comparison for Run17

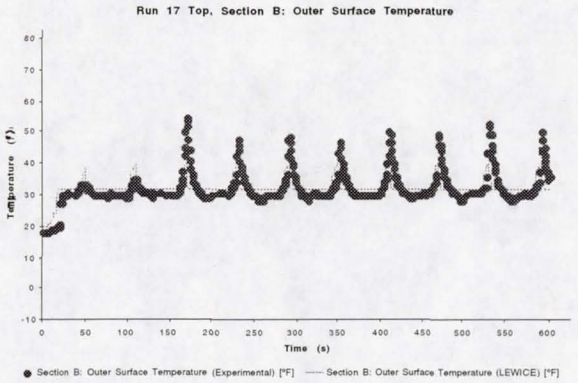

FIGURE 16. Turbulent Section "B" Surface Temperature Comparison for Run17

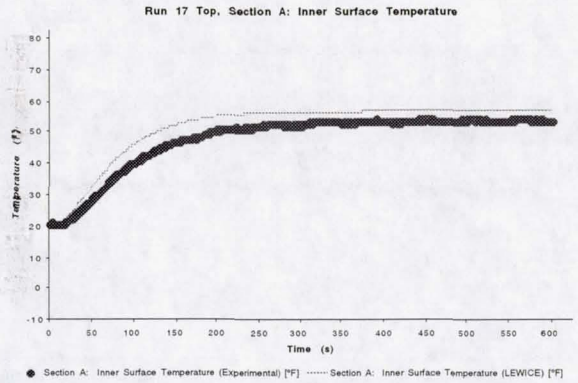

FIGURE 14. Turbulent Parting Strip Substrate Temperature Comparison for Run17

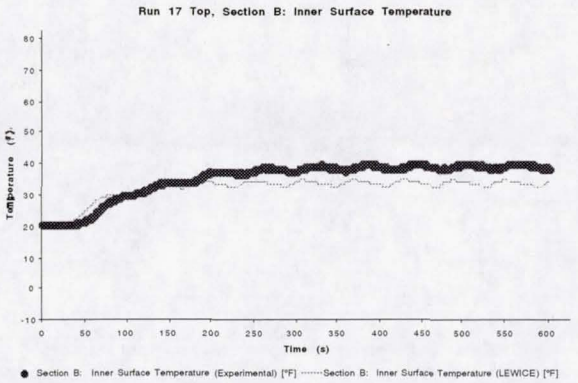

FIGURE 17. Turbulent Section "B" Substrate Temperature Comparison for Run17

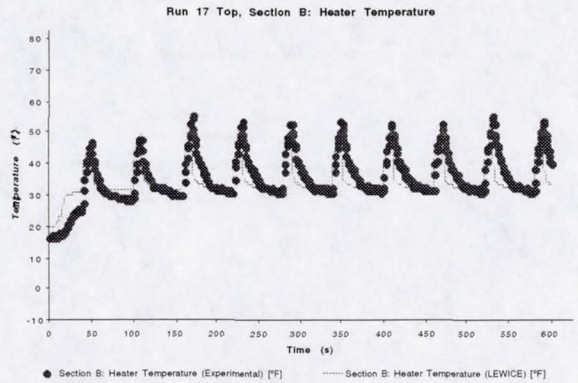

FIGURE 15. Turbulent Section "B" Heater Temperature Comparison for Run17

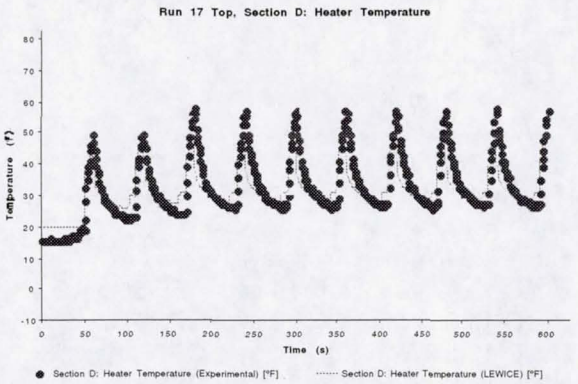

FIGURE 18. Turbulent Section "D" Heater Temperature Comparison for Run17

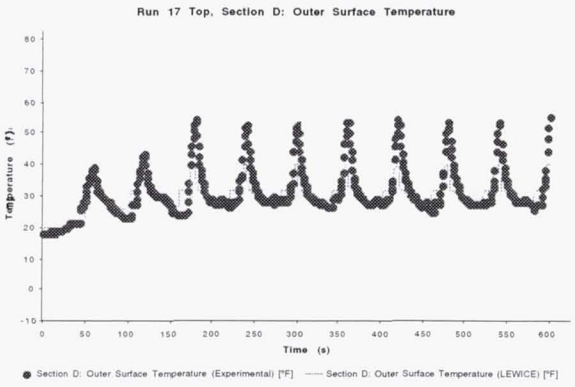

FIGURE 19. Turbulent Section "D" Surface Temperature Comparison for Run17

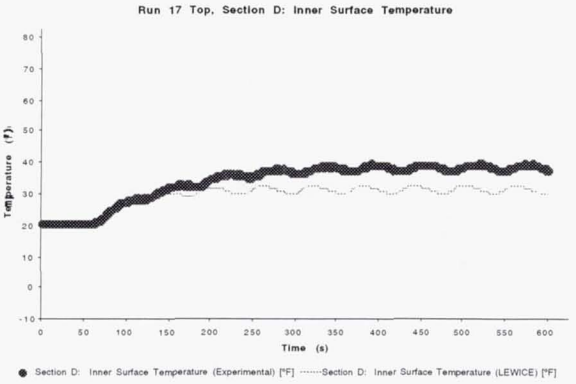

FIGURE 20. Turbulent Section "D" Substrate Temperature Comparison for Run17

TABLE 2. Conditions for Electrothermal Run 17

MVD= 20. μm
c = 0.9144 m
a = -0.5°
V_∞ = 44.7 m/s
LWC= 0.78 g/m3
T_∞ = 265.50 K
P_∞ = 100 kPa
rh = 100%
Htr. A 7.9 kW/m2 ON always
Htr. B 13.4 kW/m2 ON 10 sec. OFF 50 sec.
Htr. C 13.9 kW/m2 ON 10 sec. OFF 50 sec.
Htr. D 13.5 kW/m2 ON 10 sec. OFF 50 sec.
Htr. E 13.5 kW/m2 ON 10 sec. OFF 50 sec.
Htr. F 13.9 kW/m2 ON 10 sec. OFF 50 sec.
Htr. G 13.6 kW/m2 ON 10 sec. OFF 50 sec.
Htrs. D-G turned ON after Htrs. B&C turned OFF in the cycle.

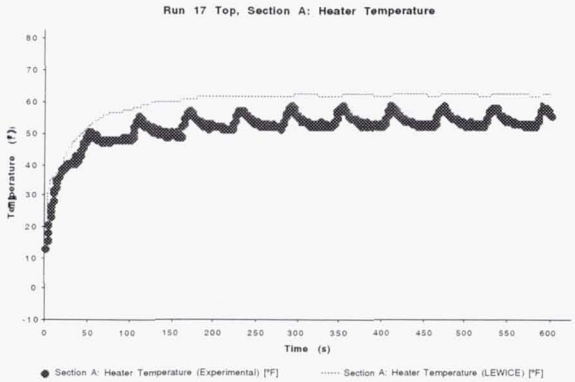

FIGURE 21. Laminar Parting Strip Heater Temperature Comparison for Run17

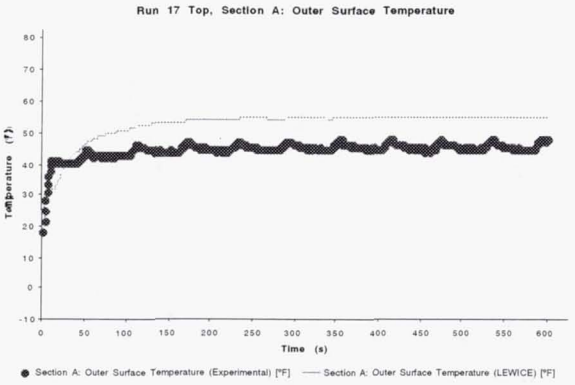

FIGURE 22. Laminar Parting Strip Surface Temperature Comparison for Run17

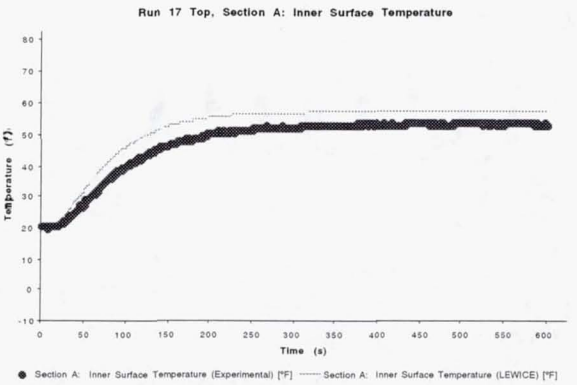

FIGURE 23. Laminar Parting Strip Substrate Temperature Comparison for Run17

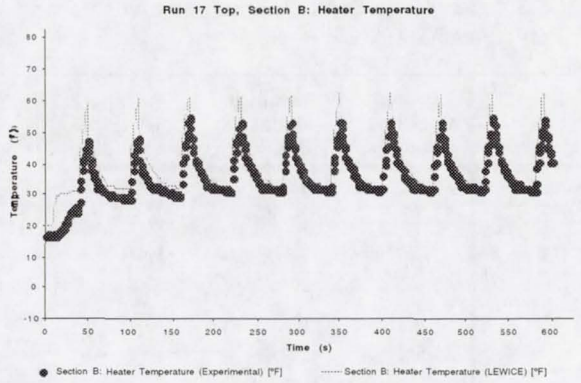

FIGURE 24. Laminar Section "B" Heater Temperature Comparison for Run17

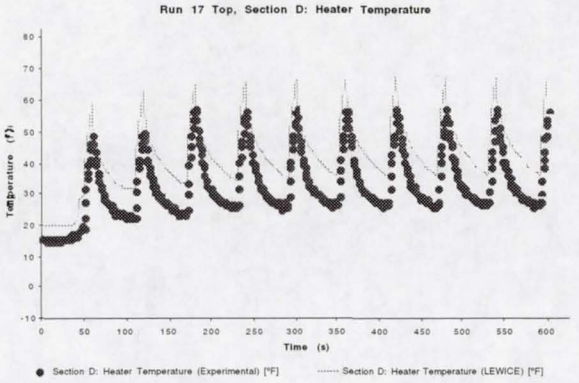

FIGURE 27. Laminar Section "D" Heater Temperature Comparison for Run17

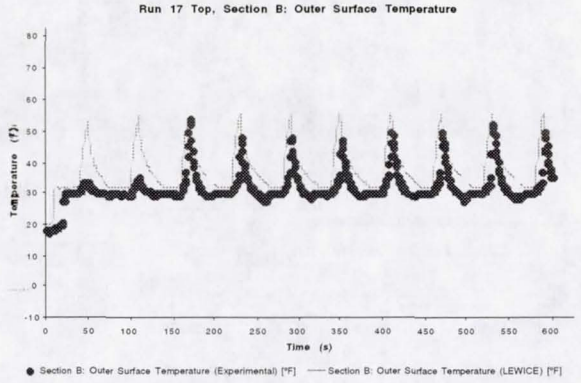

FIGURE 25. Laminar Section "B" Surface Temperature Comparison for Run17

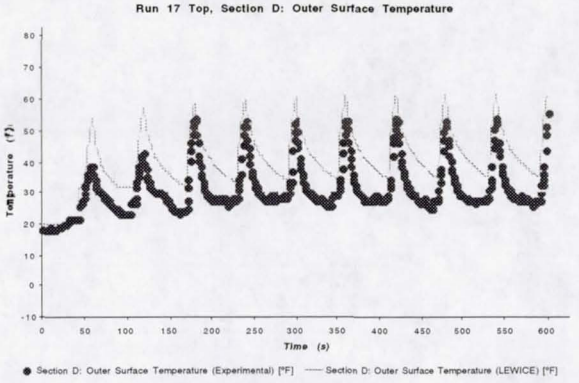

FIGURE 28. Laminar Section "D" Surface Temperature Comparison for Run17

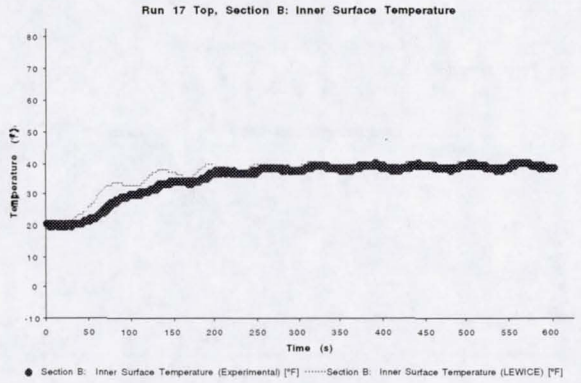

FIGURE 26. Laminar Section "B" Substrate Temperature Comparison for Run17

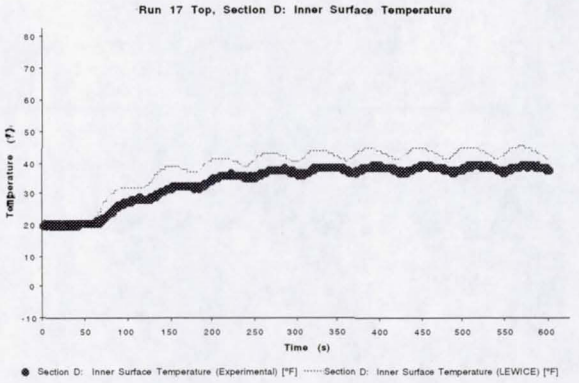

FIGURE 29. Laminar Section "D" Substrate Temperature Comparison for Run17

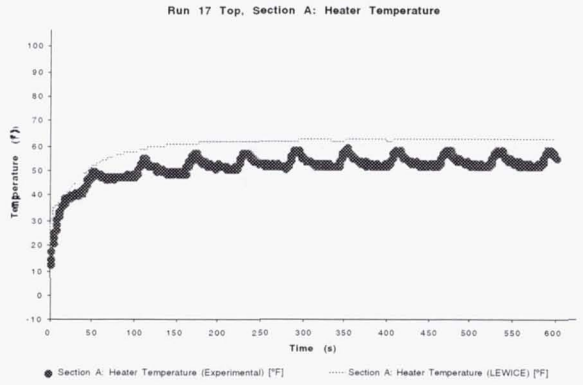

FIGURE 30. Laminar Section "A" Heater Temperature Comparison with Nodal Shedding for Run17

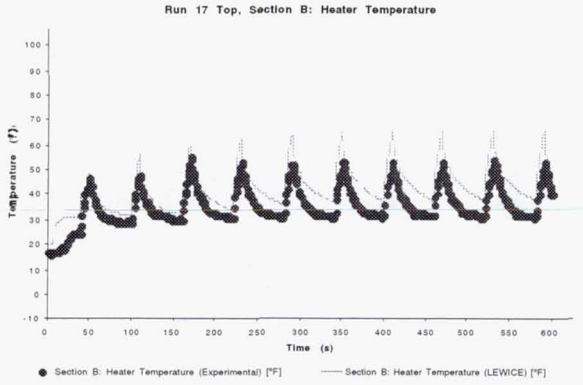

FIGURE 31. Laminar Section "B" Heater Temperature Comparison with Nodal Shedding for Run17

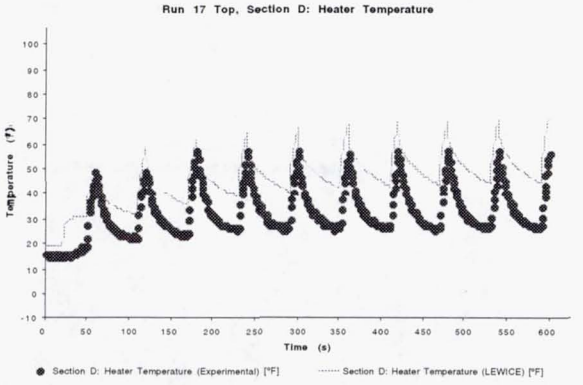

FIGURE 32. Laminar Section "D" Heater Temperature Comparison with Nodal Shedding for Run17

TABLE 3. Quantitative Comparison of Experimental and Computational Deicing Results

	Laminar, Sectional Shedding	Laminar, Nodal Shedding	Turbulent, Sectional Shedding
Overall Deicing	8.6°F, 25.7%	9.2°F, 29.6%	8.8°F, 27.2%
20°F Cases	6.5°F, 26.3%	7.3°F, 29.6%	5.9°F, 22.4%
0°F Cases	11.9°F, 24.5%	12.2°F, 29.6%	13.2°F, 29%
Evap. Anti-Icing	35°F, 22.7%	55°F, 35.6%	88.6°F, 56%
Running Wet	22.2°F, 38%	25.6°F, 44.2%	33.4°F, 53.9%

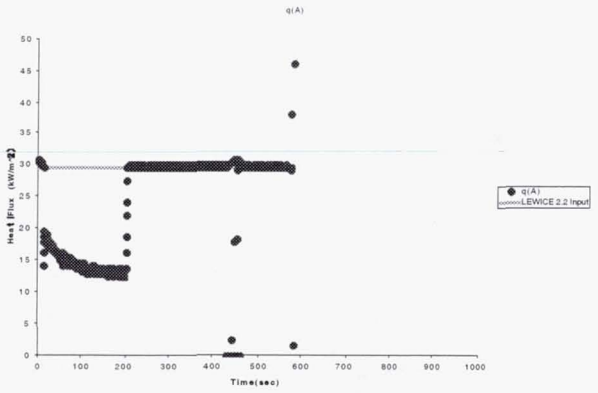

FIGURE 33. Heater Power for Run 35A, Section A

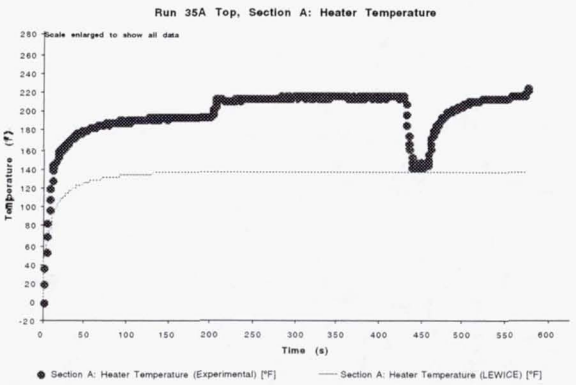

FIGURE 34. Temperature Comparison for Run 35A, Section A using Laminar Heat Transfer

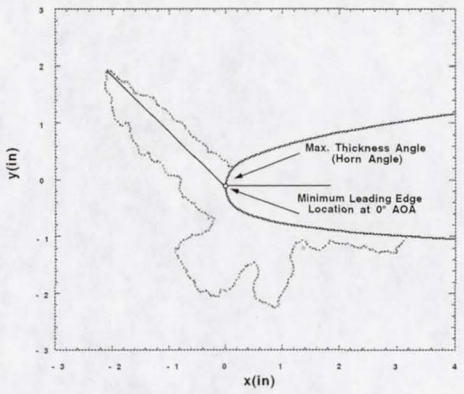

FIGURE 35. Definition of Horn Angle

TABLE 4. Comparison Of Icing Parameters for LEWICE 2.0 and LEWICE 2.2

Parameter	LEWICE 2.2 (Automated Process)	LEWICE 2.0 (Automated Process)	LEWICE 2.0 (Validation Report)
[S8] Lower Icing Limit Difference (%c)	4.8	4.8	6.1
[S7] Upper Icing Limit Difference (%c)	1.35	1.27	1.65
[S6] Leading Edge Minimum Difference (% of total thickness)	7.5	8.1	5.7
[S5] Iced Area Difference (% of total thickness * width)	10.5	10	9.9*
[S4] Lower Horn Angle Difference (degrees)	30.7	29.7	29.6*
[S3] Lower Horn Thickness Difference (% of total thickness)	14.1	14	11.7
[S2] Upper Horn Angle Difference (degrees)	22.3	20.9	16.4*
[S1] Upper Horn Thickness Difference (% of total thickness)	14.7	13	9.7

TABLE 4. Comparison Of Icing Parameters for LEWICE 2.0 and LEWICE 2.2

Parameter	LEWICE 2.2 (Automated Process)	LEWICE 2.0 (Automated Process)	LEWICE 2.0 (Validation Report)
[S3] Lower Horn Thickness Difference (% of total thickness)	14.1	14	11.7
[S2] Upper Horn Angle Difference (degrees)	22.3	20.9	16.4*
[S1] Upper Horn Thickness Difference (% of total thickness)	14.7	13	9.7

* The LEWICE 2.0 validation report used different equations to calculate these parameters, therefore the values cannot be directly compared.